Accepted Manuscript

Process optimization for producing hierarchical porous bamboo-derived carbon materials with ultrahigh specific surface area for lithium-sulfur batteries

Yinglin Yan, Mangmang Shi, Yiqi Wei, Chao Zhao, Matt Carnie, Rong Yang, Yunhua Xu

PII: S0925-8388(17)33993-2

DOI: 10.1016/j.jallcom.2017.11.212

Reference: JALCOM 43905

To appear in: *Journal of Alloys and Compounds*

Received Date: 26 July 2017

Revised Date: 14 November 2017

Accepted Date: 18 November 2017

Please cite this article as: Y. Yan, M. Shi, Y. Wei, C. Zhao, M. Carnie, R. Yang, Y. Xu, Process optimization for producing hierarchical porous bamboo-derived carbon materials with ultrahigh specific surface area for lithium-sulfur batteries, *Journal of Alloys and Compounds* (2018), doi: 10.1016/j.jallcom.2017.11.212.

Process optimization for producing hierarchical porous bamboo-derived carbon materials with ultrahigh specific surface area for Lithium-sulfur batteries

Yinglin Yan[a, *], Mangmang Shi[a], Yiqi Wei[a], Chao Zhao[b, **], Matt Carnie[b], Rong Yang[a], Yunhua Xu[a]

[a] Institute of Chemical Power Sources, School of Materials Science and Engineering, Xi'an University of Technology, 5 South Jinhua Road, Xi'an, 710048, People's Republic of China

[b] Materials Research Centre, College of Engineering, Swansea University, Bay Campus, Fabian Way, Swansea SA1 8EN, UK

Abstract

Bamboo derived porous carbon materials, as inexpensive and environmentally friendly, microporous material sources, have been attracting enthusiastic attention for energy storage applications. In this work three different processes were employed to prepare three types of bamboo derived porous carbon materials. Among them, the sample prepared via a one-step activation method delivered the largest total pore volume (1.146 $cm^3 g^{-1}$) and the largest specific surface area (1824.4 $m^2 g^{-1}$) owning to a hierarchical porous structure. After the sample was used to encapsulate sulfur (S) to prepare carbon/S composite as cathodes for Li-S batteries. The composite loaded with 58.5 wt.% S exhibited a high initial capacity of 1453 mAh g^{-1} at a rate of 0.1 C (1 C = 1675 mA g^{-1}). A reversible capacity of 255 mAh g^{-1} was maintained after 500 cycles at 1 C with a capacity decay rate of only 0.0016% per cycle. This suggests that the bamboo derived porous carbon could be a promising conductive carbon matrix for carbon/S composite cathodes in Li–S batteries.

Keywords Lithium-sulfur batteries; bamboo strip; biomass; high specific surface area.

*Corresponding author:

Dr. Yinglin Yan,

School of Materials Science and Engineering,

Xi'an University of Technology,

5 South Jinhua Road, Xi'an, 710048, People's Republic of China,

Tel: +86 29 82312107

Fax: +86 29 82312107

E-mail address: yyl3550@xaut.edu.cn

**The second corresponding author

Dr. Chao Zhao,

Materials Research Centre, College of Engineering,

Swansea University

Bay Campus, Fabian Way, Swansea SA1 8EN

E-mail address: Chao.Zhao@swansea.ac.uk

1. Introduction

During the last several decades, the rapid development of new energy systems, electric vehicles and consumer appliances has seen lithium ion battery (LIB) technology come to dominate the battery market [1,2]. More recently, lithium-sulfur (Li-S) batteries have received ever-increasing attention due to their high theoretical capacity (1675 mAh g^{-1}), high energy density (2600 Wh kg^{-1}), extremely low cost, and low toxicity [3,4]. However, there are still several challenges to be overcome, such as: 1) the poor electronic conductivity of bulk sulfur and sulfides limits electron transport in the cathode and leads to low active material utilization[5,6]; 2) the noticeable volume expansion (up to 80%) of the sulfur cathode during cycling processes leads to pulverization and collapse of the cathode materials[7–10]; 3) the dissolution of polysulfide intermediates, such as Li_2Sx ($4 \leq x \leq 8$), gives rise to shuttle phenomenon that sulfur species transport back and onward between electrodes, contributing to low Columbic efficiency and active material loss[11–13]. To date, focused efforts have been made to solve the above problems, involving introducing of conductive carbon materials (e.g. hollow carbon [8], porous carbon[9], disordered carbon nanotubes[14], double-shelled hollow carbon spheres[15], spherical ordered mesoporous carbon nanoparticles[16]) to improve the electronic conductivity; nitrogen-doping[2,17,18]; or combining polar metallic oxides[19] to suppress the shuttle effect of polysulfide. Despite these efforts however, many challenges still exist in order to achieve practical applications. [20]

Biomass derived conductive carbon materials have attracted increasing attention on account of their abundance, sustainability, and easy accessibility[21]. Biomass-derived carbon materials, such as bamboo waste[22], banana peel[23], corncob waste[24], and peanut skins[25], have good electronic conductivity, large specific surface area, and large pore volume accommodating severe volume changes of the sulfur cathode during charge/discharge processes. Bamboo is one of the most abundant natural resources due to fast growth and short maturity cycle, and is a promising biomass resource. The bamboo stem, possesses a unique well-connected three-dimensional microtexture, and contains the three structural polymers: cellulose, hemicellulose, and lignin. It can be carbonized into a hierarchical porous carbonaceous structure at 800 □, which possesses large surface area, high conductivity, well-connected and a highly ordered structure[26,27]. Recently, bamboo leaves[21], bamboo waste[22], and commercially obtained bamboo carbon[28] were utilized to synthesize sulfur/carbon (S/C)composite as a cathode material for Li-S batteries and deliver increased performance. Carbonizing the bamboo culm, usually involves several days of pretreatment of the raw materials

(grinding natural bamboo and soaking with KOH solution [22]). The resultant high specific surface area and large pore volume can contribute to accommodating high sulfur content, shortening the distance for charge transport and providing more reactive sites to improve the utilization of active sulfur material. Despite this however, the specific surface area and pore volume of bamboo derived carbon materials in the reported literature so far should be promoted further [21,22,28,29].

It is well-known that KOH plays an important role in the formation of porous networks and opening up the layered graphitic structure[28]. In order to optimize the preparation process and shorten the preparation time, three different processes were employed to synthesize bamboo-derived carbon materials in this work. Firstly, bamboo strips were carbonized under high temperature by direct pyrolysis carbonization. The direct pyrolysis bamboo-derived carbon (DBC) was prepared by this method. The DBC and KOH were mixed and carbonized under high temperature for second time in what is known as the two-step activation strategy. The corresponding product is named two-step activated bamboo-derived carbon (TBC). Finally, the one-step activation strategy involves mixing bamboo strips with KOH, and carbonizing under high temperature in a single step. This product is named one-step activated bamboo-derived carbon (OBC). The three different processes are illustrated in Scheme 1. Among them, the one-step activation strategy is the most convenient and timesaving method and its product, the OBC material, exhibits a graphene-like morphology with ultrahigh specific surface area and large total pore volume. The S/C composite cathode prepared from OBC delivers a high specific capacity, long-term cycling performance, and good rate capability, which may be attributed to the abundant pore microstructures with ultrathin-wall structure. The one-step activation strategy is a promising preparation method for bamboo-derived activated carbon material, for use as a conductive matrix for cathode composite in Li-S batteries.

2. Experimental Section

2.1. Materials Preparation

2.1.1. Synthesis of bamboo-derived carbon materials

The bamboo culms were collected from bamboo gardens in Xi'an University of Technology (Xi'an, China) and firstly cut into bamboo strips (length: ~5 mm; width: ~3 mm; thickness: ~0.5 mm) using a penknife. The bamboo strips were cleaned with distilled water and alcohol and then dried at 60 □ in the oven for 24 h before

further processing.

Method a: direct pyrolysis carbonization

The dry bamboo strips were transferred to a tube furnace with nitrogen flow and preheated to 300 □ for 30 min to remove free and bound water, then annealed at 800 □ for 1 h with a heating rate of 5 □ min^{-1}. The obtained product was washed thoroughly with distill water and alcohol several times. Finally, the washed product was dried in air at 80 □ for 12 h then fully ground into small particles which we denote as DBC particles in this article.

Method b: two-step activation

The as-obtained DBC particles were mixed with KOH (w/w=1:4) and stirred for 1 h. After the initial mixing process, 20ml distill water was added into the above mixed solution with mechanical agitation for 5 h at 80 □. The product was then dried in an oven at 80 □ for 24 h. Subsequently, the mixture was transferred to a tube furnace with nitrogen flow and preheated to 300 □ for 30 min, then annealed at 800 □ for 1 h with a heating rate of 5 □ min^{-1}. The product was cooled to room temperature and then washed with 1 M HCl solution, followed by washing with distilled water several times until the pH of the mixture solution was 7. The particles were then dried in air at 80 □ for 12 h. Finally, the product was fully ground into small particles and named as TBC.

Method c: one-step activation

The dry bamboo strips were directly mixed with KOH (w/w=1:4) and stirred for 1 h. After adding 20 mL distilled water, the solution was heated to 80 □ with stirring for 5 h and then dried in an oven at 80 □ for 24 h. The mixture was transferred to a tube furnace with nitrogen flow and preheated to 300 □ for 30 min, then annealed at 800 □ for 1 h at a heating rate of 5 □ min^{-1}. After being treated, the residue was washed with 1 M HCl solution and distill water until the pH was 7. Finally, the washed product was dried in air at 80 □ for 12 h and fully ground into small particles. The obtained sample was named as OBC.

2.1.2. Preparation of carbon/sulfur composites

The sulfur/carbon composites were prepared by a conventional melting diffusion strategy. Briefly, the sublimed sulfur powders and the as-prepared bamboo-derived carbon were mixed (weight ratio of 6 : 4) and ground in an agate mortar, then sealed in a vacuum glass tube. The tube was heated at 158 □ for 10 h in a muffle furnace under an N_2 atmosphere. After cooling to room temperature, the S/DBC, S/TBC, and S/OBC

composites were obtained.

2.2. Materials Characterization

The microstructure and morphology of all samples were characterized by X-ray powder diffraction (XRD) analysis using a D/MAX2550V x-ray diffractometer (Rigaku, Japan) with Cu $K_{\alpha 1}$ radiation (k = 1.5406 Å) at 40 kV and 40 mA, a JSM-6700F scanning electron microscopy (SEM, JEOL, Japan), and JEM-2100F transmission electron microscopy (TEM, JEOL, Japan). Energy dispersive X-ray spectroscopy (EDX) analysis and element mapping were obtained from JSM-6700F (JEOL, Japan). The specific surface areas and pore volumes of all samples were measured by the Brunauer-Emmett-Teller (BET) method using nitrogen adsorption and desorption isotherms on a Micromeritics (JW-BK122-B, JWGB SCI. & Tech., China). Pore size distribution plot is obtained by Horvath-Kawazoe method from the adsorption branch of the N_2 adsorption/desorption isotherms. The S content in the C/S composites were determined by thermogravimetric analysis (TGA) carried out under an N_2 atmosphere from room temperature to 500 °C on a Series Q500 instrument (TA Instruments, USA).

2.3. Electrochemical measurements

All samples were mixed with conductive graphite (KS-6) and polyvinylidene fluoride (PVDF) at a weight ratio of 70:20:10 and then N-2-methylpyrrolidinone (NMP) was added dropwise to form a slurry. The homogeneous slurry was cast onto aluminum current collectors, followed by vacuum drying at 55 °C for 12 h, and punching into round cathodes. The CR2025-type coin cells were assembled in an argon-filled glove box where water and oxygen were both below 0.1 ppm. Lithium metal was chosen as the counter electrode and a polypropylene membrane (Celgard 2300) served as the separator. The electrolyte was 1 M bis (trifluoromethane)sulfonylimide lithium (LiTFSi) with 1 wt.% $LiNO_3$ as an additive dissolved in the mixture of dimethoxyethane (DME) and 1, 3 -dioxolane (DOL) (1:1 by volume) (Beijing Institute of Chemistry, Beijing, China). Galvanostatic charge/discharge tests were carried out using a Neware battery tester in the voltage range of 1.5 - 3.0V (vs Li^+/Li). The specific capacity values were calculated on the basis of the mass of the active sulfur (1 C = 1675 mA g^{-1}). All of the electrochemical tests were performed at room temperature. Cyclic voltammetry (CV) was performed on an electrochemical workstation (CHI 660E, Shanghai, China) at a scanning rate of 0.1 mV s^{-1} between 1.5 and 3.0 V versus Li^+/Li. Electrochemical impedance spectroscopy (EIS) was conducted on the same instrument at frequencies between 100 kHz and 0.01 Hz with an amplitude of 5 mV.

3. Results and discussion

The TGA results of bamboo strips under Ar atmosphere are shown in Fig. S1. The weight loss from room temperature to 200 □ is 3.23 wt.% due to the evaporation of water. The weight loss of 70.05 wt.% from 200 to 800 □ arises from the decomposition and oxidation of the small and large organic molecules such as cellulose, hemicellulose, and lignin [21]. The XRD patterns of three kinds of bamboo-derived carbon materials (DBC, TBC, and OBC) are displayed in Fig. 1(a). As can be seen, all the XRD patterns are composed of two broad diffraction peaks located at ~24 ° and ~44 ° assigning to the (002) and (100) facets of the hexagonal carbon, which reveal that the three carbon materials exist in a mixed state of amorphous and crystalline phase. Moreover, the peak intensity of OBC is lower than that of DBC and TBC, suggesting that the amorphous degree of OBC is higher than the other samples, which could be due to the graphitic planes being broken by the creation of more porous structure with smaller fragments. Raman spectroscopy is used to characterize the graphitization of OBC and the result is shown in Fig. 1(b). There are two major Raman bands located at 1328 and 1594 cm^{-1}. which are identified as the disorder-induced D band and the in-plane vibrational G band, respectively [29]. The peak height ratio of I_D/I_G is 1.09,which is higher than that of reported bamboo-derived carbon materials [22,29,30], indicating a higher amorphous degree and more defect sites in OBC framework.

Nitrogen adsorption and desorption measurements (at 77 K) were employed to analyze the differences in the micropores and mesoporous properties of the as-synthesized carbon materials, which gives an insight into the activation effect of KOH on the mesoporous properties of the bamboo-derived carbon material. The nitrogen adsorption/desorption isotherms and corresponding pore size distribution of DBC, TBC, and OBC are displayed in Fig. 2. In the adsorption/desorption isotherms (Fig. 2(a)), the DBC have a BET surface area of 153.1 $m^2 g^{-1}$ and pore volume of 0.107 $cm^3 g^{-1}$ those are the lowest of the three bamboo-derived carbon materials. The TBC shows a type I isotherm (a Langmuir-type isotherm) in Fig. 2(b) indicating the characteristic microporous structure. The BET area and micropore volume of the TBC are 823.5 $m^2 g^{-1}$ and 0.357 $cm^3 g^{-1}$, respectively. An intricate isotherm mixed with type I and type IV is observed from the OBC sample, indicating the sample possesses both microporous and mesoporous structural features. The BET specific surface area is 1824.4 $m^2 g^{-1}$ and the pore volume is 1.146 $cm^3 g^{-1}$, which demonstrates that OBC has much higher BET surface areas than that of DBC and TBC due to the generation of more micro- and meso- pores during the pyrolysis carbonization process. The corresponding pore size distribution was calculated by the Saito-Foley method and is displayed in

the inset of Fig. 2(c). It is worth noting that the OBC has a main pore size distribution peak located at 0.85 nm and two smaller peaks ranging from 2 to 4 nm, and that the OBC material possesses a hierarchical porous microstructure. All the above testing results and corresponding information reported in other references are listed in Table 1. According to Table 1, it is clear that the OBC sample exhibits the highest BET area (1824.4 m^2 g^{-1}) and the largest micropore volume (1.146 cm^3 g^{-1}). It has been observed that high specific surface area and large pore volume can contribute to accommodating high sulfur content, which can shorten the distance for charge transport and provide more reactive sites to improve the utilization of active sulfur material. Moreover, the hierarchical porous microstructure can not only supply facile transport channels for Li-ions, but also efficiently retain the intermediates in the cathodic chamber to reduce the loss of the active material and prevent the polysulfides shuttling to the anodic compartment[29].

The morphology of the bamboo-derived carbon materials had been further investigated by digital camera, SEM, and TEM. The corresponding images are displayed in Fig.3. Pristine bamboo strip exhibits a vascular bundle structure composing of hollow cylindrical cells linked together as shown in the digital image (Fig. 3(a)). As displayed in the SEM image (Fig. 3(b)), there are only a few holes that can be found on the surface of the DBC sample particles. The holes are much less frequent than the raw bamboo material arising to incomplete carbonization. Additionally, abundant pores retained from the raw bamboo can be obviously observed in the TBC sample (shown in Fig. 3(c)). The formation of these pores is due to activation by KOH. However, as can be seen in the SEM images (Fig. 3(d, e)) and TEM image (Fig. 3(f)) of OBC material, the morphology was changed thoroughly. In the low-magnification SEM image (Fig. 3(d)), the particles previously observed have given way to abundant graphene-like thin sheets which are also observed in the high-magnification SEM image (Fig. 3(e)). The TEM image (Fig. 3(f)) further confirms the graphene-like morphology and porous microstructure of the OBC material contributing to the large specific surface area, which is consistent with the N_2 adsorption/desorption results (Fig. 2).

After sulfur is loaded into the bamboo-derived carbon material, the morphology of the S/OBC, displayed in Fig. 3(g), is clearly different from the OBC morphology observed in Fig. 3(e). The surface of OBC sheets become smoother without any observable pores on account of sulfur particles filling into the pores of OBC. In order to further verify the distribution of sulfur in the composite, EDS mapping analysis was carried out on the S/OBC composite, and the corresponding elemental mapping images for sulfur and carbon are shown in Fig.

3(h) and (i), respectively. The bright red spots represent sulfur and the green spots represent carbon. We observe a uniform distribution of sulfur throughout the whole area, concurrently with a uniform coverage of carbon. The results demonstrate that the sulfur and the carbon are alternate distribution in the scan region, which illustrates the majority of the sulfur has been well impregnated in the pore structure of the OBC. The homogeneous distribution of sulfur in the composite can improve the performance of Li–S batteries.

XRD patterns and TGA curves of pure sulfur, S/DBC, S/TBC, and S/OBC composites are displayed in Fig. 4. The sublimed sulfur shows strong sulfur diffraction peaks (Fig. 4(a)) (JCPDF NO. 08-0247). All XRD patterns of S/C composites in Fig. 4(a) show sulfur signals and the intensity is decreasing step-by-step from S/DBC to S/TBC and S/OBC, implying that sulfur is in a highly dispersed state inside the pores[9]. The corresponding TGA curves (Fig. 4(b)) show that the sulfur mass loading of S/OBC, S/TBC, and S/DBC composites are 58.5 wt. %, 57.6 wt. %, and 53.4 wt. % respectively. The S/OBC composite has the highest sulfur mass loading, which is due to the fact that the OBC exhibits the largest specific surface area and pore volume giving it the strongest adsorption ability.

The electrochemical properties of the S/DBC, S/TBC and S/OBC cathodes are evaluated using CR2025-type coin cells. Fig. 5(a-c) displays the galvanostatic charging-discharging profiles of S/DBC, S/TBC, and S/OBC cathodes. All charging-discharging profiles were measured at a rate of 0.1 C. The discharging curves represent the lithiation capacities of the S/DBC, S/TBC and S/OBC cathodes and the 1^{st} discharging capacities are 696, 846, and 1453 mAh g^{-1} respectively. Afterward the capacities of the samples are attenuating along with the cycling number increasing. There are two obvious plateaus present in the discharge curves, corresponding to the two different reduction processes for the S/C composite cathodes. Noteworthily, the second plateau of the 1st discharge curves are lower in voltage than subsequent cycles and possess long tails which disappear in subsequent cycles, which we attribute to the decomposition of $LiNO_3$ additives. This can promote the formation of a stable passivation film on the Li metal anode and effectively suppress the redox shuttle of polysulfides. However, $LiNO_3$ was reduced irreversibly on the cathode surface at voltages lower than 1.6 V, as a result of the growing of passivation film on the Li anode. When $LiNO_3$ was exhausted, the cell impedance and charge-discharge polarization can be optimized[31]. In addition, the S/OBC cathode possesses longer and higher than those of S/DBC, S/TBC cathodes and have a large increased capacity from 1.9 V to 1.7 V, which circled in Fig. 5(c) can be attributed to the deep reduction from short chain polysulfides to the final

products of Li_2S and Li_2S_2. The enhanced performances can be attributed to the hierarchical porous microstructure of the OBC matrix, which can provide large pore volume for sulfur infiltration, a mesoporous structure for rapid ion transport, and thus high power performance and small pores for reducing polysulfide dissolution [32].

Fig. 5(d) shows the cycling performance of the S/DBC, S/TBC and S/OBC cathodes. As can be seen, the discharge capacities decay relatively fast for the initial 10 cycles, which is mainly due to the loss of active sulfur and the dissolution of long chain polysulfides into the electrolyte, the decay rates eventually slow down and a reversible capacity of 291 mAh g^{-1}, 401 mAh g^{-1}, and 711 mAh g^{-1}corresponding to S/DBC, S/TBC and S/OBC cathodes still remained after 50 cycles with a stable Coulombic efficiency close to 100 %. The S/OBC cathode exhibits the best cycling performance and although the initial capacity of the S/TBC cathode is lower than that of the S/DBC sample, the discharge capacity retention of the S/TBC cathode is 57.6 %, which is higher than that of the S/DBC (34.4%). The porous microstructure plays a very important role in the cycling performance. The micropores in TBC provide higher adsorption power to reduce polysulfide dissolution. The hierarchical porous microstructure of OBC not only possesses higher adsorption power, but also provides higher surface area available for good electrical contact with sulfur, which enhances the utilization. Thus, the S/OBC composites cathode exhibits the best cycling performance.

The S/DBC, S/TBC, and S/OBC composites cathodes cycled at different current rates increased from 0.1 to 1 C and returned to 0.1 C (1 C = 1675 mA g^{-1}) in the voltage range of 1.5 – 3.0 V are shown in Fig.5(e). For S/OBC composites cathodes, an initial discharge capacity of 1481 mA g^{-1} was obtained at 0.1 C, after further cycles at 0.2, 0.5, and 1 C rates, it showed stable reversible capacities about 867, 665, and 561 mA g^{-1}, respectively. When the rate returned to 0.1 C, 691 mA g^{-1} was obtained again. It is clearly observed the rate performances of the S/DBC, S/TBC cathodes are inferior to the S/OBC cathode because the hierarchical architecture of mesoporous and macro-pores in OBC can promote the penetration of electrolyte into the porous carbon. Consequently, it shortens the diffusion path for the ingress/egress of Li^+ to react with sulfur [32]. The good rate performance reveals that the interfacial charge-transfer process and lithium-ion diffusion in the S/OBC nanocomposite are critically favorable for electrochemical reaction of sulfur.

It is noteworthy from the Fig.5(e) that the capacity of S/OBC composite at 1 C is very stable. The long-term (500 cycles) cycling performance of the S/OBC cathode at 1 C is presented in Fig. 5(f), which

indicates the outstanding electrochemical stability compared to the other composite cathodes. Relatively high reversible capacities of, 382 mAh g^{-1} after 100 cycles, and 255 mAh g^{-1} after 500 cycles, at 1 C are obtained from the Fig. 5(f). The average capacity attenuation from 100th cycle to 500th cycle is about 0.33 mAh g^{-1} per cycle, namely the capacity decay rate is only 0.0016% per cycle. We compare the electrochemical performance of the S/OBC cathode (the current work) with other related state-of-the-art S cathodes based on bamboo-derived carbon host materials, which is depicted in Table 3. The S/OBC composite shows excellent electrochemical performance, such as the second-high initial capacity, the third rate performance, and the longest cycle life with useable capacity.

Cyclic voltammetry (CV) testing was conducted to investigate the electrochemical mechanisms of the as-prepared S/OBC cathode materials. Fig. S2 shows the CV profiles of the S/OBC cathode in the voltage window between 1.0 and 3.4 V versus Li^+/Li at a scanning rate of 0.1 mV s^{-1}. For the 2nd cycle, there are four reduction peaks in the cathode reduction profiles. They are located at approximately 2.3 V, 2.0 V, 1.7 V and 1.4 V, corresponding to the reduction processes of elemental sulfur to long chain lithium polysulfides (Li_2S_x, $4 < x < 8$) and the conversion of long chain lithium polysulfides to short chain lithium polysulfides, to insoluble Li_2S, respectively. In the subsequent anodic scan, one asymmetric oxidation peak is observed at around 2.4 V and attributed to the conversion of lithium sulfides to polysulfides and sulfur [33,34]. Meanwhile for the 50^{th} cycle, the positions of the reduction peaks are transferred to higher voltages due to the activation of cathode materials. In addition, the integral areas of the reduction peaks are decreased confirming the loss of the capacity. In the subsequent anodic scan, two weak peaks with reduced area are observed which implies that the S/OBC cathode material is activated gradually during the cycling process and the electrical conductivity of the active substance is improved as well.

To further understand the improved electrochemical performances of S/OBC cathode materials, the EIS (Fig. 6) of the S/DBC, S/TBC and S/OBC cathodes before discharge and after 50 cycles were measured to study the dynamics for lithium insertion and extraction during cycling. Before discharging, the impedance spectra in Fig. 6(a) are composed of a short inclined line at the low frequency region representing semi-infinite diffusion of soluble lithium polysulfide in the electrolyte (Warburg impedance) and a semicircle at the medium-to-high frequency attributing to the charge transfer process at the interface between the electrolyte and sulfur electrode (R_{ct}). The high-frequency intercept on the real axis represents

the resistance of the electrolyte (R_e). [28] However, after 50 cycles, the impedance spectra in Fig. 6(b) added a new small resistance, including two depressed semicircles followed by a long sloping line. The straight line is still attributed to the diffusion of Li ions in the matrix (Warburg impedance). The semicircle in the high frequency range is related to the solid-electrolyte-interface (SEI) film caused by the formation of Li_2S (or Li_2S_2) on the surface of the carbon cathode (R_s). The semicircle in the medium frequency region reflects the R_{ct} [22]. The equivalent circuit models for analyzing impedance spectra are shown in the inset of Fig. 6(a) and Fig. 6(b), respectively. CPE is a constant phase element which is used instead of capacitance and W_c is the Warburg impedance due to the diffusion of the polysulfides within the Cathode [28]. The fitted R_e, R_{ct}, R_s values of the cells according to the equivalent circuit are shown in Table 2.

All the R_e of three samples are less than 10 Ω, attributing to the good electronic conductivity of bamboo-derived carbon materials. After 50 cycles, the R_{ct} of all the samples decrease dramatically, indicating that an active process may be necessary for the penetration of the electrolyte into the electrodes[10]. Simultaneously, the semicircle in the high frequency range arises with cycling, which should be a result of the irreversible deposition and aggregation of insoluble Li_2S and Li_2S_2 on the surface of bamboo-derived carbon materials. The R_s of S/DBC is larger than those of the other samples, which may be due to a thicker deposited layer. Noticeably, no matter before or after cycling, the sample made from S/OBC cathode possesses lowest impedance because of the great electrical conductivity of OBC. The transportation of Li-ions becomes much easier as the cycle number increase, which in turn benefits the high rate capability of the cathode during long cycling as a result of the infiltration of the electrolyte and chemical activation process for the dissolution and redistribution of the active materials [35]. Consequently, the S/OBC composite cathode demonstrates the best performance, attributing to the hierarchical porous microstructure, which give rise to the highest sulfur utilization and least shuttle phenomenon.

4. Conclusions

Three types of Bamboo-based activated carbon materials (DBC, TBC, OBC) have been successfully synthesized by the simple pyrolysis carbonization method with or without KOH activation. The OBC sample prepared via one-step activation strategy possesses a hierarchical porous structure, giving rise to a large pore volume of 1.146 $cm^3\ g^{-1}$ and a high specific surface area of up to 1824.4 $m^2\ g^{-1}$. All three carbon

materials were mixed with sulfur material to fabricate carbon-sulfur composites (S : C = 6 : 4) as the cathode materials in Li-S batteries. The S/OBC composite cathode exhibited extraordinary electrochemical performance due to the hierarchical porous structure. The large total pore volume and excellent specific surface area play key roles in encapsulating sulfur and adsorbing polysulphides, which facilitated electrical contact between the sulfur and the conductive carbon framework during the charge/discharge process and reduced the shuttle phenomenon during cycling. In addition, the porous structure allows a greater degree of electrolyte infiltration into the cathode material. Therefore, the S/OBC sample delivers a high initial capacity of 1453 mAh g^{-1} at 0.1 C and high reversible capacities of 382 mAh g^{-1} after 100 cycles and 255 mAh g^{-1} after 500 cycles at 1 C. Consequently, the OBC could replace the commercial activated carbon and other more expensive carbonaceous materials, for use in energy storage devices, due to its easy availability, low cost, and excellent surface area. Our work suggests that the natural resource of common bamboo could be an essential raw material for future energy storage applications.

Acknowledgment

This work was supported by the International Science and Technology Cooperation Program of China (Nos. 2015DFR50350), the National Natural Science Founda- tion of China (no. 51702256), Basic Research Plan of Natural Science Funded by Shaanxi Science and Technology Department (Nos. 2017JQ5055), Science and technology project of Shaanxi Province (2017GY-160).

References

[1] C. Huang, D. Ai, L. Wang, X. He, LiFePO 4 Crystal Growth during Co-precipitation, Int. J. Electrochem. Sci. 11 (2016) 754–762.

[2] J. Zhang, L. Zhang, S. Yang, D. Li, Z. Xie, B. Wang, Y. Xia, F. Quan, Facile strategy to produce N-doped carbon aerogels derived from seaweed for lithium-ion battery anode, J. Alloys Compd. 701 (2017) 256–261. doi:10.1016/j.jallcom.2017.01.082.

[3] Y. Son, J.S. Lee, Y. Son, J.H. Jang, J. Cho, Recent Advances in Lithium Sulfide Cathode Materials and Their Use in Lithium Sulfur Batteries, Adv. Energy Mater. 5 (2015) 1–14. doi:10.1002/aenm.201500110.

[4] P.G. Bruce, S.A. Freunberger, L.J. Hardwick, J.-M.M. Tarascon, Li–O2 and Li–S batteries with high energy storage, Nat. Mater. 11 (2011) 172–172. doi:10.1038/nmat3237.

[5] A. Manthiram, Y. Fu, S. Chung, C. Zu, Y. Su, Rechargeable Lithium–Sulfur Batteries, Chem. Rev. 114 (2014) 11751–11787. doi:10.1021/cr500062v.

[6] A. Manthiram, Y. Fu, Y. Su, Challenges and Prospects of Lithium À Sulfur Batteries, Acc. Chem. Res. 46 (2013) 1125–1134. doi:10.1021/ar300179v.

[7] Y. Yang, G. Zheng, Y. Cui, Nanostructured sulfur cathodes, Chem. Soc. Rev. 42 (2013) 3018–3032. doi:10.1039/c2cs35256g.

[8] G. Ma, Z. Wen, J. Jin, Y. Lu, X. Wu, M. Wu, C. Chen, Hollow polyaniline sphere@sulfur composites for prolonged cycling stability of lithium–sulfur batteries, J. Mater. Chem. A. 2 (2014) 10350. doi:10.1039/c4ta00483c.

[9] S. Zhao, C. Li, W. Wang, H. Zhang, M. Gao, X. Xiong, A. Wang, K. Yuan, Y. Huang, F. Wang, A novel porous nanocomposite of sulfur/carbon obtained from fish scales for lithium–sulfur batteries, J. Mater. Chem. A. 1 (2013) 3334. doi:10.1039/c3ta01220d.

[10] W.G. Wang, X. Wang, L.Y. Tian, Y.L. Wang, S.H. Ye, In situ sulfur deposition route to obtain sulfur-carbon composite cathodes for lithium-sulfur batteries, J. Mater. Chem. A. 2 (2014) 4316–4323. doi:10.1039/c3ta14459c.

[11] F. Qin, K. Zhang, J. Fang, Y. Lai, Q. Li, Z. Zhang, J. Li, High performance lithium sulfur batteries with a cassava-derived carbon sheet as a polysulfides inhibitor, New J. Chem. 38 (2014) 4549–4554. doi:10.1039/c4nj00701h.

[12] W. Chen, T. Qian, J. Xiong, N. Xu, X. Liu, J. Liu, J. Zhou, X. Shen, T. Yang, Y. Chen, C. Yan, A New Type of Multifunctional Polar Binder: Toward Practical Application of High Energy Lithium Sulfur Batteries, Adv. Mater. 29 (2017) 1605160. doi:10.1002/adma.201605160.

[13] X. Ji, K.T. Lee, L.F. Nazar, A highly ordered nanostructured carbon-sulphur cathode for lithium-sulphur batteries., Nat. Mater. 8 (2009) 500–506. doi:10.1038/nmat2460.

[14] H. Yao, G. Zheng, W. Li, M.T. McDowell, Z. Seh, N. Liu, Z. Lu, Y. Cui, Crab shells as sustainable templates from nature for nanostructured battery electrodes, Nano Lett. 13 (2013) 3385–3390. doi:10.1021/nl401729r.

[15] S.H. Chung, A. Manthiram, Carbonized eggshell membrane as a natural polysulfide reservoir for highly reversible Li-S batteries, Adv. Mater. 26 (2014) 1360–1365. doi:10.1002/adma.201304365.

[16] Y. Liang, Z. Li, R. Fu, D. Wu, Nanoporous carbons with a 3D nanonetwork-interconnected 2D ordered mesoporous structure for rapid mass transport, J. Mater. Chem. A. 1 (2013) 3768. doi:10.1039/c3ta01307c.

[17] J. Ou, L. Yang, Z. Zhang, X. Xi, Honeysuckle-derived hierarchical porous nitrogen, sulfur, dual-doped carbon for ultra-high rate lithium ion battery anodes, J. Power Sources. 333 (2016) 193–202. doi:10.1016/j.jpowsour.2016.09.163.

[18] F. Zheng, D. Liu, G. Xia, Y. Yang, T. Liu, M. Wu, Q. Chen, Biomass waste inspired nitrogen-doped porous carbon materials as high-performance anode for lithium-ion batteries, J. Alloys Compd. 693 (2016) 1197–1204. doi:10.1016/j.jallcom.2016.10.118.

[19] F. Zhou, L.-T. Song, L.-L. Lu, H.-B. Yao, S.-H. Yu, Titanium-Carbide-Decorated Carbon Nanofibers as Hybrid Electrodes for High Performance Li-S Batteries, ChemNanoMat. 2 (2016) 937–941. doi:10.1002/cnma.201600227.

[20] Y. Yuan, K. Amine, J. Lu, R. Shahbazian-Yassar, Understanding materials challenges for rechargeable ion batteries with in situ transmission electron microscopy, Nat. Commun. 8 (2017) 15806. doi:10.1038/ncomms15806.

[21] Y. Li, L. Wang, B. Gao, X. Li, Q. Cai, Q. Li, X. Peng, K. Huo, P.K. Chu, Hierarchical Porous Carbon Materials Derived from Self-Template Bamboo Leaves for Lithium–Sulfur Batteries, Electrochim. Acta. 229 (2017) 352–360. doi:10.1016/j.electacta.2017.01.166.

[22] Y. Cheng, S. Ji, Y. Liu, J. Liu, High sulfur loading in activated bamboo-derived porous carbon as a superior cathode for rechargeable Li-S batteries, Arab. J. Chem. (2015). doi:10.1016/j.arabjc.2015.10.001.

[23] E.M. Lotfabad, J. Ding, K. Cui, A. Kohandehghan, W.P. Kalisvaart, M. Hazelton, D. Mitlin, High-density sodium and lithium ion battery anodes from banana peels, ACS Nano. 8 (2014) 7115–7129. doi:10.1021/nn502045y.

[24] J. Guo, J. Zhang, F. Jiang, S. Zhao, Q. Su, G. Du, Microporous carbon nanosheets derived from corncobs for lithium–sulfur batteries, Electrochim. Acta. 176 (2015) 853–860. doi:10.1016/j.electacta.2015.07.077.

[25] H. Wang, W. Yu, J. Shi, N. Mao, S. Chen, W. Liu, Biomass derived hierarchical porous carbons as

high-performance anodes for sodium-ion batteries, Electrochim. Acta. 188 (2016) 103–110. doi:10.1016/j.electacta.2015.12.002.

[26] X. zhou, L. Li, S. Dong, X. Chen, P. Han, H. Xu, J. Yao, C. Shang, Z. Liu, G. Cui, A renewable bamboo carbon/polyaniline composite for a high-performance supercapacitor electrode material, J. Solid State Electrochem. 16 (2012) 877–882. doi:10.1007/s10008-011-1435-3.

[27] P. McKendry, Energy production from biomass (part 1): overview of biomass, Bioresour. Technol. 83 (2002) 37–46. doi:10.1016/S0960-8524(01)00118-3.

[28] X. Gu, Y. Wang, C. Lai, J. Qiu, S. Li, Y. Hou, W. Martens, N. Mahmood, S. Zhang, Microporous bamboo biochar for lithium-sulfur batteries, Nano Res. 8 (2014) 129–139. doi:10.1007/s12274-014-0601-1.

[29] X. Gu, C. Lai, F. Liu, W. Yang, Y. Hou, S. Zhang, A conductive interwoven bamboo carbon fiber membrane for Li–S batteries, J. Mater. Chem. A. 3 (2015) 9502–9509. doi:10.1039/C5TA00681C.

[30] H. Chen, D. Liu, Z. Shen, B. Bao, S. Zhao, L. Wu, Functional Biomass Carbons with Hierarchical Porous Structure for Supercapacitor Electrode Materials, Electrochim. Acta. 180 (2015) 241–251. doi:10.1016/j.electacta.2015.08.133.

[31] Z. Li, L. Yuan, Z. Yi, Y. Sun, Y. Liu, Y. Jiang, Y. Shen, Y. Xin, Z. Zhang, Y. Huang, Insight into the electrode mechanism in lithium-sulfur batteries with ordered microporous carbon confined sulfur as the cathode, Adv. Energy Mater. 4 (2014) 1–8. doi:10.1002/aenm.201301473.

[32] B. Ding, C. Yuan, L. Shen, G. Xu, P. Nie, X. Zhang, Encapsulating sulfur into hierarchically ordered porous carbon as a high-performance cathode for lithium-sulfur batteries, Chem. - A Eur. J. 19 (2013) 1013–1019. doi:10.1002/chem.201202127.

[33] N. Jayaprakash, J. Shen, S.S. Moganty, A. Corona, L.A. Archer, Porous hollow carbon@sulfur composites for high-power lithium-sulfur batteries, Angew. Chemie - Int. Ed. 50 (2011) 5904–5908. doi:10.1002/anie.201100637.

[34] H.L. Wu, L.A. Huff, A.A. Gewirth, In situ raman spectroscopy of sulfur speciation in lithium-sulfur batteries, ACS Appl. Mater. Interfaces. 7 (2015) 1709–1719. doi:10.1021/am5072942.

[35] D. Yu, L. Dai, Self-assembled graphene/carbon nanotube hybrid films for supercapacitors, J. Phys. Chem. Lett. 1 (2010) 467–470. doi:10.1021/jz9003137.

Figure captions

Scheme 1. Schematic illustration of the preparation of the bamboo derived porous carbon materials (OBC, PBC, and TBC).

Fig. 1. (a) XRD patterns of DBC, TBC, and OBC and (b) Raman spectrum of OBC

Fig. 2. Nitrogen adsorption-desorption isothermal curves and pore size distributions of (a) DBC, (b) TBC, and (c) OBC.

Fig. 3. (a) Digital image of bamboo strips. SEM images of DBC (b), TBC (c). (d and e) Low and high-magnification SEM images of OBC. (f) TEM image of OBC. (g-i) EDS map of the S/OBC composite.

Fig. 4. (a) XRD patterns of pure S, S/DBC, S//TBC, and S/OBC composites. (b) Thermogravimetric analysis (TGA) curves of pure S, OBC material, and S/DBC, S//TBC, S/OBC composites from room temperature to 500 □ at a heating rate of 5 □ min^{-1} under Ar.

Fig. 5. Galvanostatic charge and discharge curves of the S/DBC(a), S/TBC(b) and S/OBC (c) cathodes for Li-S batteries cycled between 1.5 and 3.0 V versus Li/Li^+. (d) Cycling performance of the S/DBC, S/TBC, and S/OBC cathodes at 0.1 C. (e) Rate capability of the S/DBC, S/TBC, and S/OBC cathodes. (f) Long-term cycling performance of the S/OBC cathodes at a 1 C rate (1 C = 1675 mA g^{-1}).

Fig. 6. The Nyquist plots and corresponding equivalent circuit model (a) before discharge and (b) after 50 cycles of the Li-S cells with the S/DBC, S/TBC, and S/OBC cathodes.

Table list

Table 1. BET surface area, pore volume and average pore size of bamboo-derived carbon materials obtained in this work and other references.

Table 2. Impedance parameters simulated from the equivalent circuits.

Sample	BET surface area (m^2 g^{-1})	Pore volume (cm^3 g^{-1})	Average pore size (nm)	Reference
DBC	153.1	0.107	4.092	this work
TBC	823.5	0.411	4.187	this work
OBC	1824.4	1.146	3.638	this work
HPCMs	284	0.6	-	[21]
A_BC	1565.4	0.95	1.5-5	[22]
T_BC	791.80	0.380	0.75	[28]
BCFs	776.07	0.33	0.75	[29]
NBKBC	171.5	-	-	[30]

Table 2. Impedance parameters simulated from the equivalent circuits.

Sample	Cycle number	Resistance (ohm)		
		R_e	R_{ct}	R_s
S/DBC	1st	10.5	259.8	-
	50th	6.3	21.5	26.1
S/TBC	1st	9.9	236.5	-
	50th	9.5	22.6	10.9
S/OBC	1st	8.2	172.5	-
	50th	6.9	10.4	9.5

Sample	Initial capacity	Cycling Stability	Rate Capability	Reference
OBC	1453 mAh g^{-1} at 0.1 C	711 mAh g^{-1} at 50 cycles at 0.1 C 382 mAh g^{-1} at 100 cycles at 1 C 255 mAh g^{-1} at 500 cycles at 1 C	561 mA g^{-1} at 1C	this work
HPCMs	1487 mAh g^{-1} at 0.05 C	707 mAh g^{-1} after 200 cycles at 1 C	649 mAh g^{-1} at 2C	[21]
A_BC	1160 mAh g^{-1} at 0.1 C	710 mAh g^{-1} after 100 cycles at 0.2 C	580 mAh g^{-1} at 1 C	[22]
T_BC	1295 mAh g^{-1} at 0.1 C	756 mAh g^{-1} after 50 cycles at 0.1 C	410 mAh g^{-1} at 1 C	[28]

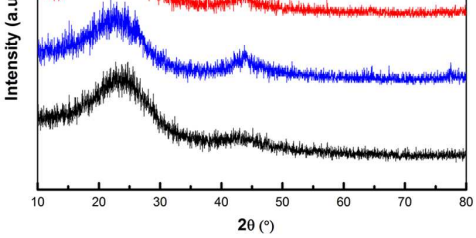

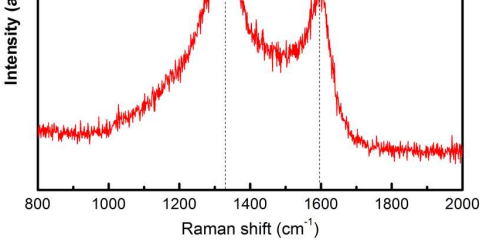

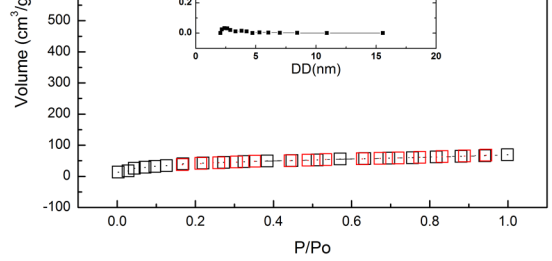

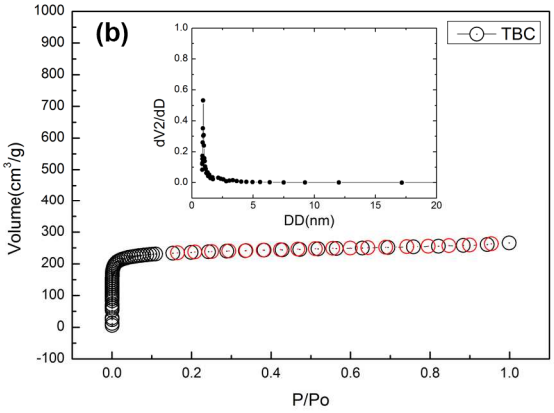

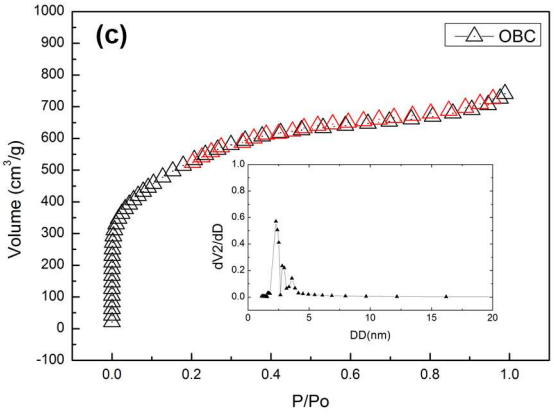

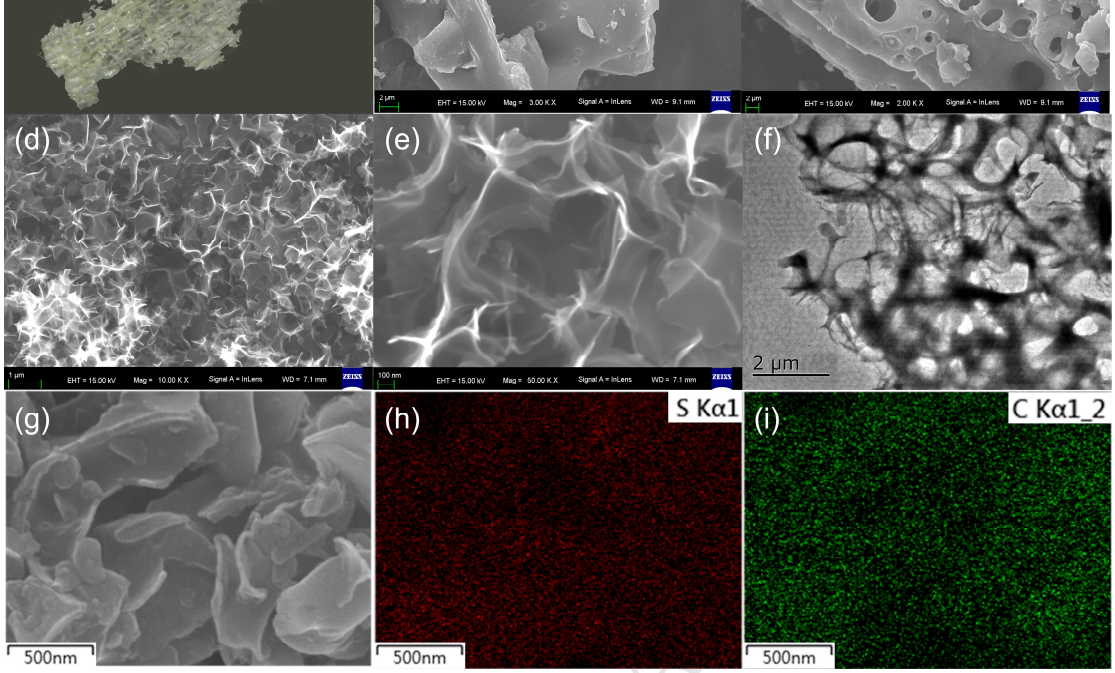

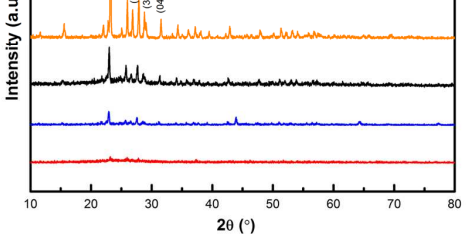

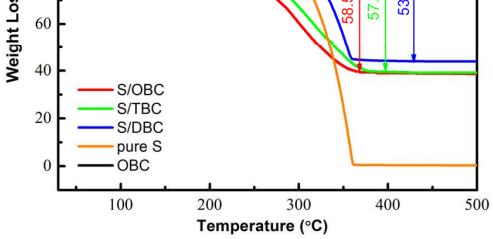

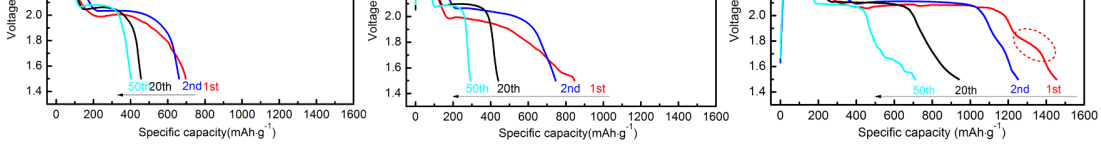
Voltage
Specific capacity(mAh·g-1)
50th
20th
2nd
1st

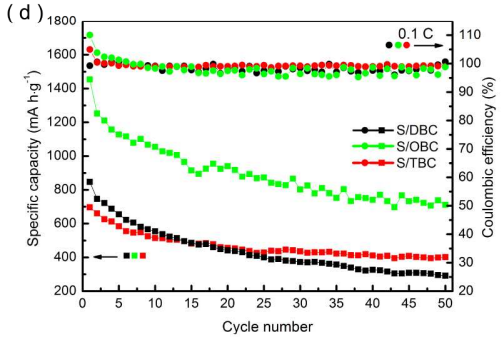
(d)
0.1 C
S/DBC
S/OBC
S/TBC
Specific capacity (mA h·g-1)
Coulombic efficiency (%)
Cycle number

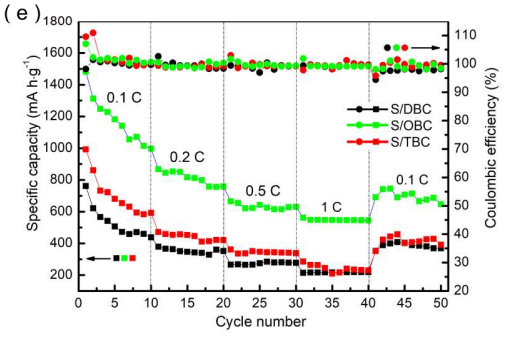
(e)
0.1 C
0.2 C
0.5 C
1 C
0.1 C
S/DBC
S/OBC
S/TBC
Specific capacity (mA h·g-1)
Coulombic efficiency (%)
Cycle number

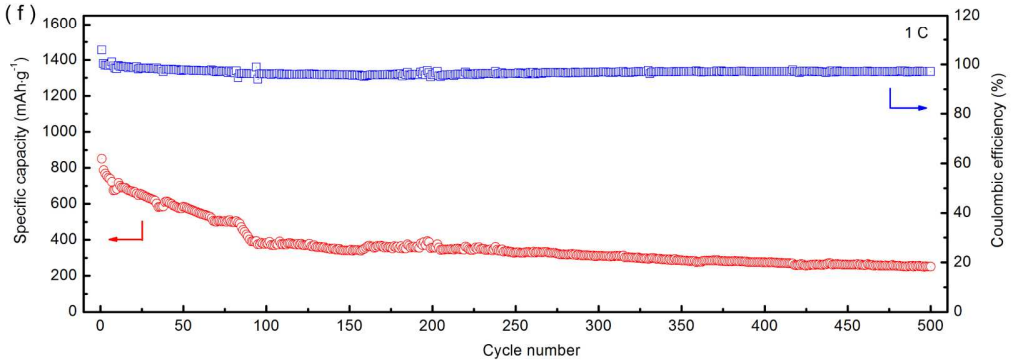
(f)
1 C
Specific capacity (mAh·g-1)
Coulombic efficiency (%)
Cycle number

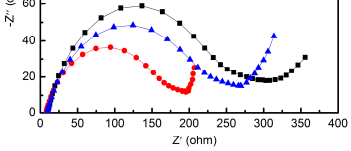

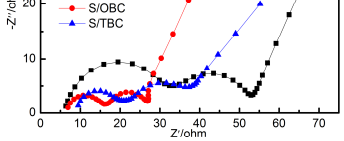

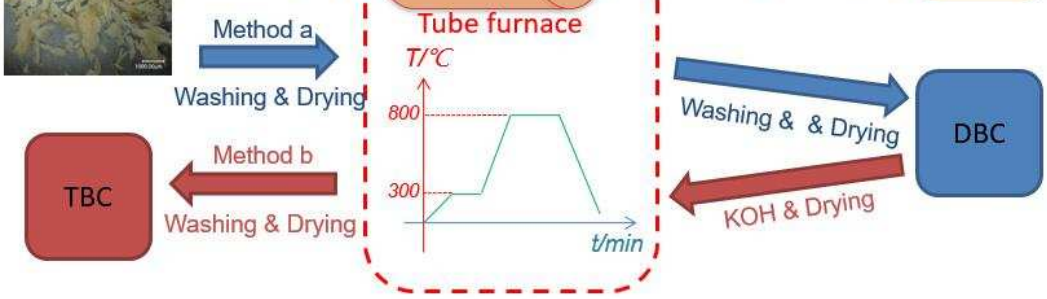

> A bamboo-derived carbon material with hierarchical porous structure was prepared;

> The OBC material possesses an ultrahigh specific surface area;

> The OBC material possesses a large total pore volume;

> The electrochemical performance of S/OBC composite was significantly enhanced.